Fitting EXAFS data using molecular dynamics outputs and a histogram approach

Stephen W. T. Price, Nicholas Zonias, Chris-Kriton Skylaris, Timothy I. Hyde, Bruce Ravel, and Andrea E. Russell

Phys. Rev. B **85**, 075439 — Published 29 February 2012

DOI: 10.1103/PhysRevB.85.075439

Fitting EXAFS data using molecular dynamics outputs and a histogram approach

Stephen W.T. Price[1], Nicholas Zonias[1], Chris-Kriton Skylaris[1], Timothy I. Hyde[2], Bruce Ravel[3] & Andrea E. Russell[1]**

1 School of Chemistry, University of Southampton, Highfield, Southampton, SO17 1BJ, UK

2 Johnson Matthey Technology Centre, Blounts Court, Sonning Common, Reading RG4 9NH, UK

3 National Institute of Standards and Technology, 100 Bureau Drive MS 8520, Gaithersburg MD 20899, USA

*corresponding authors

Abstract

The estimation of particle diameter of metal nanoparticles by the analysis of EXAFS data from coordination numbers is non-trivial, particularly for particles smaller than 5 nm in diameter, for which the under-coordination of surface atoms becomes an increasingly significant contribution to the average coordination number. These under-coordinated atoms have increased degrees of freedom over those within the core of the particle, which results in an increase in the degree of structural disorder with decreasing particle size. This increase in disorder however is not accounted for by the standard means of EXAFS analysis, where each coordination shell is fitted with a single bond length and disorder term. In addition, the surface atoms of nanoparticles have been observed to undergo a greater contraction than those in the core, further increasing the range of bond distances. Failure to account for this structural change results in an increased disorder being measured and, therefore, a lower apparent coordination number and corresponding particle size are found. Here we employ molecular dynamics (MD) simulations of a range of nanoparticle sizes to determine each of the nearest neighbour bond lengths, which were then binned into a histogram to construct a radial distribution function (RDF). Each bin from the histogram was considered to be a single scattering path and subsequently used in fitting the EXAFS data obtained for a series of carbon supported platinum nanoparticles. These MD based fits are compared with those obtained using a standard fitting model using Artemis and the standard model with the inclusion of higher cumulants, which has previously been used to account for the non-Gaussian distribution of neighbouring atoms around the absorber. The results from all three fitting methods were converted to particle sizes and compared with those obtained from TEM and XRD measurements. We find that the use of molecular dynamics simulations resulted in an improved fit over both the standard and cumulant models, in terms of both quality of fit and correlation with the known average particle size.

I Introduction

It has been shown that for highly disordered systems, EXAFS underestimates coordination number and thus particle size when compared with the theoretical coordination number based on size determination from other experimental techniques[1-4]. Similarly, when cross-correlating EXAFS with other techniques, such as TEM and XRD[5, 6], EXAFS gives smaller sizes. The failure to accurately measure the coordination number is due to a failure to account for the high degree of disorder present. The most common approach to analysing the EXAFS involves quantifying the atom-atom pair

distribution extracted from the data by approximating it to a Gaussian or near-Gaussian distribution. This allows for the determination of an average coordination number, relative position from the absorber and the mean square relative disorder, MSRD (also called σ^2 or the EXAFS Debye Waller term), of the absorbing atoms at that distance to be measured. If the Gaussian distribution becomes skewed, sharpened or flattened, additional terms (known as higher cumulants) can be added to the fitting parameters to account for this disorder[7-9], although the use of these has limitations.

A Anharmonicity

In an ideal crystalline monometallic system, at 0 K, there would be only one bond length throughout. Zero point motion, however, causes a slight variation in the bond length. Defects within a bulk system give rise to structural (static) disorder, as does decreasing the size down to the nanometre scale. Increasing the temperature increases the amount of thermal (dynamic) disorder within the system. The Debye temperature is the temperature above which the material behaves classically and where thermal vibrations are more important than quantum effects. Below this temperature, an increase in disorder produces a variation in the nearest neighbour bond length measured, that is modelled as a Gaussian distribution, and is known as the pair or radial distribution function (RDF)[10]. This is done traditionally to help reduce the number of variables in the EXAFS fitting process. When analysing particles by EXAFS, near-neighbour interactions can be parameterised as a 1D anharmonic potential based on the interatomic distance (**Equation 1**), where *a*, *b*, and *c* are the coefficients of $\psi(r)$.

$$\psi(r) = \frac{1}{2}ar^2 + br^3 + cr^4$$

Equation 1

Many parameters in the EXAFS equation, such as the disorder and coordination number, are highly correlated. As all of the individual inter-atomic distances cannot be measured independently of each other, this distribution is assumed. The width of which is equivalent to the MSRD factor in a traditional *k* space calculation of the EXAFS spectrum[11]. Above the Debye temperature, thermal effects increase in importance and can skew the pair distribution function from harmonic (Gaussian) to anharmonic (log-normal distribution) as a result of dynamic disorder. Structural defects or distortions will also have an effect on the bond length distribution, and can split the single distribution into a bi- or even tri-modal distribution. One significant example of this for nanoparticles is the case of surface atoms. Surface atoms behave differently from core atoms as they are only partially coordinated, and so are not constrained to stay close to their nominal lattice positions. This can result in a contraction of surface atoms towards the core to minimise the surface energy, which is true both for bulk materials[12] and nanoparticles[13]. These termination effects are present in both the bond length distribution and the disorder[13], as surface atoms rearrange to reduce the surface energy, whether by smoothing electron density[14] or a change in the metal-metal bond[15], and can be likened to surface tension. For bulk materials, this surface effect is negligible as the bulk contribution dominates.

With nanoparticles below 5 nm, the proportion of surface atoms is approximately 25%, rising to over 75% below 2 nm and therefore they contribute significantly to the average bond length, as well as being increasingly dominant in the EXAFS signal. With many of the atoms shifted towards shorter bond distances (surface), but the core atoms remaining (more or less) as they were, the radial distribution function will move away from a Gaussian distribution towards a multi-modal distribution, as a result of strucutral disorder. The assumption of a Gaussian distribution in the "standard" EXAFS model breaks down in systems with high disorder, whether through thermal effects or size effects. This results in errors in bond lengths, coordination numbers and disorder terms[1, 11, 16, 17]. This is a

limitation of the technique, as in disordered systems these errors tend to be exaggerated, resulting in particles appearing smaller than they are in reality, manifest by lower average coordination numbers than would be predicted by the true particle size.

B Cumulant Expansions

An early approach to compensate for anharmonicity in EXAFS was to introduce higher order cumulants into the analysis. Initially developed in 1983 by Bunker[18], and implemented as the log ratio method, the introduction of higher cumulants provided a means to address this problem of a non-Gaussian distribution. Cumulant expansions are written in terms of moments of the anharmonic potential $\psi(r)$ (**Equation 1**), and evaluated in terms of a, b and c; these being the parameters used to determine the fit. The cumulants are written as:

$$\Delta R = C_1 \approx \frac{-3bk_BT}{a^2}\left[1+\frac{k_BT}{a^2}\left(\frac{45b^2}{a}-32c\right)\right] \qquad \textbf{Equation 2}$$

$$\sigma^2 = C_2 \approx \frac{k_BT}{a}\left[1+\frac{k_BT}{a^2}\left(\frac{36b^2}{a}-12c\right)\right] \qquad \textbf{Equation 3}$$

$$C_3 \approx \frac{-6b(k_BT)^2}{a^3}\left[1+\frac{k_BT}{a^2}\left(\frac{144b^2}{a}-84c\right)\right] \qquad \textbf{Equation 4}$$

$$C_4 \approx \frac{(k_BT)^3}{a^4}\left[\frac{108b^2}{a}-24c\right] \qquad \textbf{Equation 5}$$

The first cumulant, C_1 (**Equation 2**), relates to the mean value of the inter-atomic distance (R), and the second cumulant, C_2 (**Equation 3**), to its variance (that is the Debye Waller term σ^2). Normally only the first two cumulants are used as they are significant for small degrees of disorder[10], and, if none of the higher order cumulants values are non-zero, the distribution is Gaussian. In highly disordered systems, like the nanoparticles studied in this work, the disorder is non-Gaussian, and so higher order cumulants are non-zero. The third cumulant, C_3 (**Equation 4**), measures the asymmetry of the radial distribution function with respect to a Gaussian distribution (**Figure 1a**), giving rise to a change in the average inter-atomic distance measured. If a positive C_3 is measured, the distance measured without its inclusion was an underestimate and vice versa. The fourth cumulant, C_4 (**Equation 5**), measures the symmetric sharpening and flattening of the radial distribution peak (**Figure 1b**), which is related to the coordination number and Debye Waller term. The inclusion of a positive C_4 will give a larger coordination number than without, and reduce the error associated with it by up to 40 %[7].

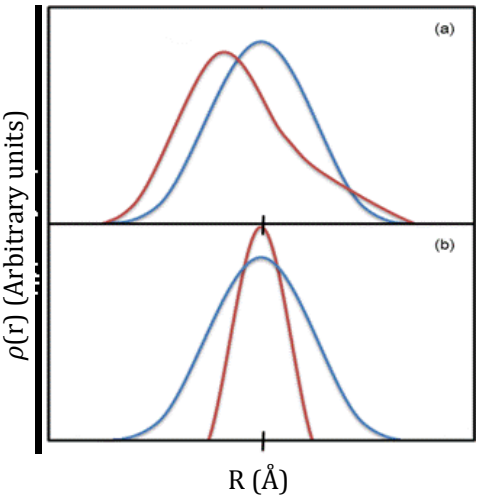

Figure 1: Schematic of effect of a) third cumulants, (C_3 - red) and b) fourth cumulants (C_4 - red) on a Gaussian distribution (blue) with variance C_2.

Low temperature measurements, in particular below the Debye temperature of a material, reduce the dynamic disorder in the system, reducing the effect of the anharmonic contribution[10], notably from the under-coordinated surface atoms. For bulk systems, this can be enough to give an accurate value of the coordination number and disorder. Complications arise due to the fact that the Debye temperature of very small particles can differ from the known bulk values[1]. Consequently, measurements must be taken at as low a temperature as possible to ensure the system is below its Debye temperature. With the dynamic disorder greatly reduced, that which is left is structural disorder due to any termination effects brought about by the size of the particles.

C Molecular Dynamic Studies of EXAFS

The inputs for both "standard" and "cumulant" EXAFS fitting of metallic particles are based on a bulk crystalline lattice where anharmonic thermal motion and surface termination effects are negligible. In nano-sized systems, there is a need for the correct treatment of the distribution of neighbours, to account for the effects of the increasingly high proportion of disordered surface atoms with decreasing particle size[19].

The "standard" and "cumulant" models fit a single distribution for each coordination shell. If the contributions from surface bonds are different enough from the core, the distribution will become bimodal and any attempt to fit a single peak over the split distribution will result in the introduction of systematic errors. A cumulant expansion which stops at either the second or fourth term introduces substantial systematic error into the fitting results due to the fact that the second or fourth term expansion is an inadequate approximation of the true distribution function. MD offers a mechanism for better approximating this distribution in the EXAFS analysis

Much prior work has been reported that addressed the accurate determination of coordination number from EXAFS, looking at the relationship between surface atom anharmonicity and particle geometry[20-23]. These theoretical studies clearly demonstrate the difference in radial position and intensity of each nearest neighbour shell as a function of the particle geometries modelled, yet still focussed on an even distribution of bond lengths from the core to the surface, with no contraction or other termination effects being accounted for.

Work has been reported where MD has been used to simulate the EXAFS, and the results compared to real structural data such as that by Okamoto[20] and Gilbert *et al.* [24, 25], although only a few previous studies have attempted to use MD to more accurately determine average coordination number from EXAFS[2, 3]. The disorder modelled in these systems, however, still remained a single pseudo-Gaussian distribution, unlike that reported here. Studies by Clausen *et al.* on nanoparticles below 5 nm diameter have been largely theoretical, although work has been done on larger particles[2, 3, 17]. Of the previous studies combining MD with EXAFS, all have been for data collected at high temperature, and so dynamic disorder dominates any fine structural disorder. As such, the disorder is pseudo-Gaussian and can be modelled using higher cumulants to account for small degrees of asymmetry within the distribution, an approach that also works well for disordered radial distributions in liquids[9, 18, 26]. Below 3 nm, the disorder is significantly non-Gaussian and so the use of higher cumulants will fail to accurately address the problem. Applying the structural information obtained from MD to real EXAFS data is needed to determine if the non-Gaussian nature of the disorder has a significant effect on the EXAFS fit, and to assess the validity of the assumption of a symmetrical distribution of bond lengths.

Most recently Yevick and Frenkel[27] have simulated increasing the degree of surface disorder on a small metallic cluster, and how this effects the RDF. As in this work, they investigated the assumption of bulk-like disorder and a symmetric bond length distribution, although as with the majority of previous studies their work was purely theoretical. One other important difference is that their work is based on a radial distortion model, multiplying the distance of each atom from the centre of the cluster by a distortion function, rather than the molecular dynamic modelling performed in this work.

The amount of information in the MD output used as the EXAFS fitting input is far larger than that in the "standard" analysis. The total number of atom-atom pair distances measured throughout the simulation makes direct fitting unmanageable due to the number of potential scattering paths. Previously, a histogram approach has been used effectively by Ravel *et al.* to model the bond length distribution in highly disordered bulk materials[28, 29]. In this approach all atom-atom pair distributions within a small range are binned into a histogram to reduce the information content of the input to a manageable size.

The work reported here compares the standard, cumulant and molecular dynamics methods for EXAFS analysis, and identifies the current limitations for each approach. Cross-correlation with XRD and TEM is used as a means to evaluate the effectiveness of each approach in determining coordination number and, therefore, an estimate of particle size.

II Experimental

A series of supported platinum nanoparticles (10, 20, 40 and 60 wt% on a commercially available high surface area graphitic support) were supplied by the Johnson Matthey Technology Centre (Sonning Common) and characterised there using XRD and TEM-EDX techniques

Pt L_{III} edge (11564 eV) EXAFS data were acquired at beam line X23A2 of the National Synchrotron Light Source, USA, using a Si(311) monochromator. The samples were prepared as boron nitride pellets and reduced under flowing H_2 for 30 minutes. Spectra were acquired in transmission mode using 20% Ar/80% N_2 filled ion chambers at temperatures from 20 to 300 K.

The XRD analysis used a Bruker AXS D8 Advance[1] diffractometer with a Ni filtered Cu Kα X-ray source. XRD patterns were collected over a scan range of 10 to 140° 2Θ with a 0.022° step size at a scan rate of 0.264° 2Θ per minute.

Powder samples for TEM-EDX were crushed between two glass slides and samples positioned onto a lacey carbon coated copper "finder" grid with the aid of a micromanipulator. The samples were examined for particle size analysis in a Tecnai F20 transmission electron microscope. Both bright field and high-resolution electron microscopy modes were used.

Classical Molecular Dynamics (MD) simulations have been performed on several Pt cluster sizes using the DL_POLY 2.0 software package[30]. The starting configurations consisted of 55, 177, 381 and 767 atoms, representing sizes of 1.39, 1.94, 2.50 and 3.05 nm respectively (**Figure 2**). The starting configurations of the clusters were based on approximately spherical geometries, assuming a complete outer shell of atoms, and were generated using the ATOMS program[31], with Pt face-centred cubic structure and a unit cell primitive vector of 3.92 Å (1 Å = 100 pm) magnitude, corresponding to the structural properties of bulk Pt.

For describing the atomic interactions, both the Gupta potential[32] and a Sutton-Chen potential[33] were used in our simulations. Each simulation was carried out within the micro-canonical (NVE) ensemble, with a time-step of 1 fs between every MD frame. The atomic forces and velocities were equilibrated for a period of 50 ps, after which a production calculation of 2 ns followed. Atom pair distribution data in the form of a radial distribution function (RDF) were collected over the production stage, after confirming that both the energy and temperature were stabilised. A very fine grid spacing (bins) between the collected RDF data for the generated histogram was used to provide a more representative interpretation of the bond length distribution, by taking surface termination effects into account.

Although the MD results reported in this work mainly refer to the simulations conducted with the Sutton-Chen force field, sample simulations using the Gupta potential were performed to allow comparison and validation of the reliability of the calculated results. Despite some discrepancies observed regarding the predicted MD oscillations, the structural features of any simulated system using both force fields are considered to be in good agreement with experimental data[34]. Within this framework, RDF results were obtained from simulations conducted at 20 K.

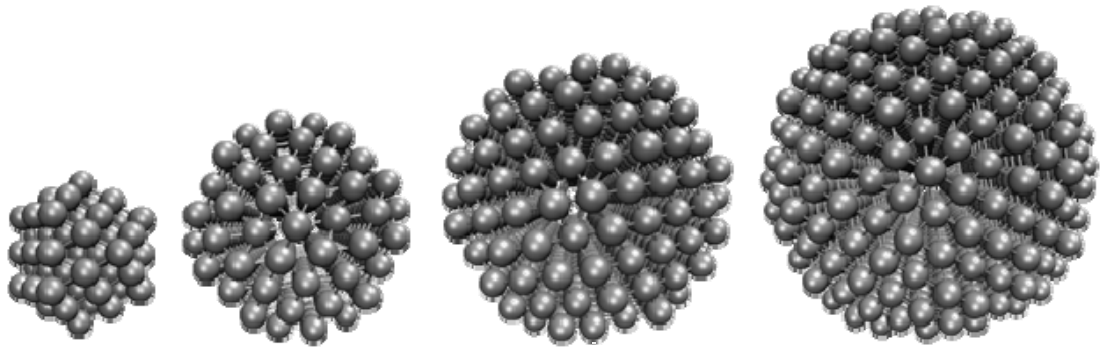

Figure 2: Starting configurations of nanoparticles used for MD simulations.

1 Any mention of commercial products is for information only; it does not imply recommendation or endorsement by NIST.

The MD output sums up all atom pair distributions thought the nanoparticle over the duration of the simulation. The histogram generated provides a more representative interpretation of the bond length distribution, taking surface termination effects into account.

III Data analysis

The acquired data was processed and analysed using the programs Athena and Artemis[35], which implement the FEFF6 and IFEFFIT codes[36, 37]. The AUTOBK method[38] was used to isolate the *k*-space EXAFS data from the raw data, and a theoretical EXAFS signal was constructed using FEFF6. Data were collected for a Pt foil prior to the nanoparticle measurements to enable determination of the amplitude reduction factor, without the which the coordination number cannot be accurately determined[39]. This was found to be 0.85 ± 0.03; all coordination numbers and subsequent results were corrected accordingly.

The EXAFS was fit up to the first coordination shell by standard means. In this work, standard analysis refers to using a bulk *fcc* structure to generate the theoretical scattering paths that FEFF calculates, and that are used to fit the experimental data to theory. None of the surface termination effects or anharmonic behaviour present in the nanoparticles are accounted for in this approach. Data were fit from 2 Å to 3.2 Å in R, 3 $Å^{-1}$ to 18 $Å^{-1}$ in *k* (cryostat data) and 3 $Å^{-1}$ to 17 $Å^{-1}$ (300 K data), with multiple *k*-weighting. The path degeneracy was also used as a fitting parameter due to the termination effects present in nanoparticles. The other fitting parameters were an isotropic expansion coefficient α, energy correction ΔE_0 and disorder σ^2. The EXAFS signal contained some noise with a low R component that could not be removed during data processing without affecting the amplitude of the data. This resulted in a slight misfit around 2 Å in R space. EXAFS determined average particle size was based on the methods of Jentys[40] and Benfield[41].

To apply the MD approach the raw EXAFS data were processed and fit to theory as with the standard approach, but instead of using *fcc* Pt as the structural model for the fit to the data, the output of the MD output was used. At each time step of the MD simulation, the atomic coordinates of the atoms in the cluster were analysed and each Pt-Pt contact distance present in the cluster was extracted. This was repeated at each time step, resulting in an ensemble consisting of the tens of thousands of Pt-Pt distances observed during the simulation. This ensemble of distances was then binned by distance into a histogram. The population of each histogram bin, then, represents the number of Pt-Pt pairs with a distance falling within that bin. The amplitudes of all histogram bins for the first coordination shell were normalised to unity. The sum of the contributions from each histogram bin, therefore, represents a single scattering atom distributed over the RDF from the MD simulation.

To compute the contribution to the EXAFS from that distribution, we began with a FEFF6 calculation on bulk Pt. This bulk Pt calculation was used to obtain a reasonable approximation of the scattering potential of the Pt atom. This computed atomic potential was used along with the distance of each bin to calculate the contribution to the EXAFS from a scatterer found at that distance. Each such contribution was weighted by the bin population. The EXAFS contribution from each histogram bin was then parameterised using the same 4 variables as in the standard approach; amplitude *N*, isotropic expansion coefficient α, energy correction ΔE_0 and disorder σ^2. A disorder term was still needed for the fits, as the simulations did not fully account for the thermal vibrations within the molecule[34]. An energy correction parameter was retained in this model as well as in the conventional and cumulant models. Although using the same value for ΔE_0 in all fitting models might result in more precise

determinations of α, fixing a parameter like ΔE_0 has the undesirable consequence of removing an important correlation with α from the fitting problem. Without reliable prior knowledge of ΔE_0, we cannot impose this constraint without sacrificing the accuracy of the determination of α.The sum of the weighted contributions from each bin represents the EXAFS signal from the entire distribution. All data were fit over a range in R between 2 and 3.2 Å, and between 3 and 18 $Å^{-1}$ in *k*.

The scatterers at the different distances within the histogram give rise to a much more complex phase relationship than that of a much simpler Gaussian distribution (**Figure 3**). Whilst the MD simulations do not perfectly model the nanoparticles[34], they provide an improvement over the standard model, and by fitting the EXAFS data with different MD simulation outputs, a means by which to evaluate the simulations ability to model real nanoparticles also becomes available.

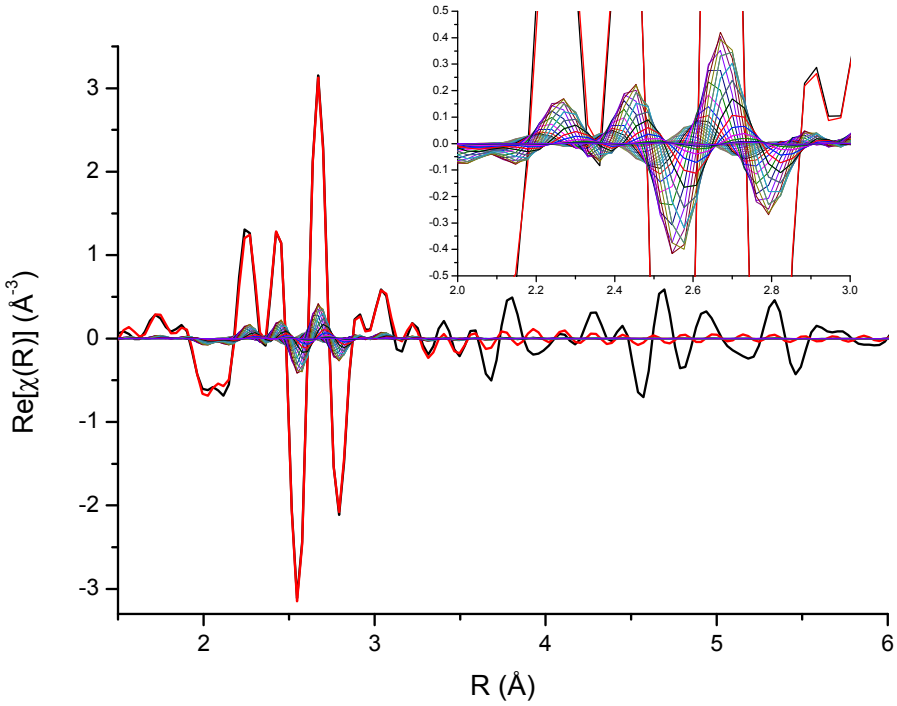

Figure 3: Fourier transform of the phase relationship between scattering paths generated from RDF output from a Sutton-Chen simulation of a 381 atom Pt cluster for the first coordination shell. Black line is 40wt% Pt/C at 20 K data, red line is the fit using the sum of the RDF scattering path; RDF scattering paths are lower amplitude multi-coloured lines, with a close-up of the first shell scattering paths in inset. The fit was performed as detailed in the Data Analysis section.

IV MD EXAFS

The histogram generated by the molecular dynamics (MD) output provides a simple representation of how the standard and cumulant approaches can fail (**Figure 4**). Basing the analysis on a Gaussian distribution for the case shown would introduce a significant systematic error into the analysis. In the standard model, the MSRD (σ^2) is used to describe the variance of the atomic displacement from the absorbing atom at distance *R*. This variance can be due to both structural disorder and thermal

vibrations - averaged out over the whole structure - and is modelled by a Gaussian or near-Gaussian distribution. In nanoparticles, such as those under study here, there is no large structure over which to average out, and so termination effects (surface contraction) are significant and result in a low R tail. Assuming the nanoparticles are nominally *fcc* in packing (as in the standard analysis model), on a very local scale, an atom pair will occasionally have an interatomic distance far larger than the standard value - i.e. 2.772 Å for Pt - giving rise to a high R tail. For particles ≥ 100 nm diameter, these tails in the distribution are insignificant, and a Gaussian approximation for the MSRD is sufficient. For nanoparticles < 10 nm diameter, the lack of long range order and large surface area to volume ratio become significant, especially with regard to termination effects. This is seen in all the MD simulations run where the largest contraction in nearest neighbour distances comes from the surface shell[13, 27].

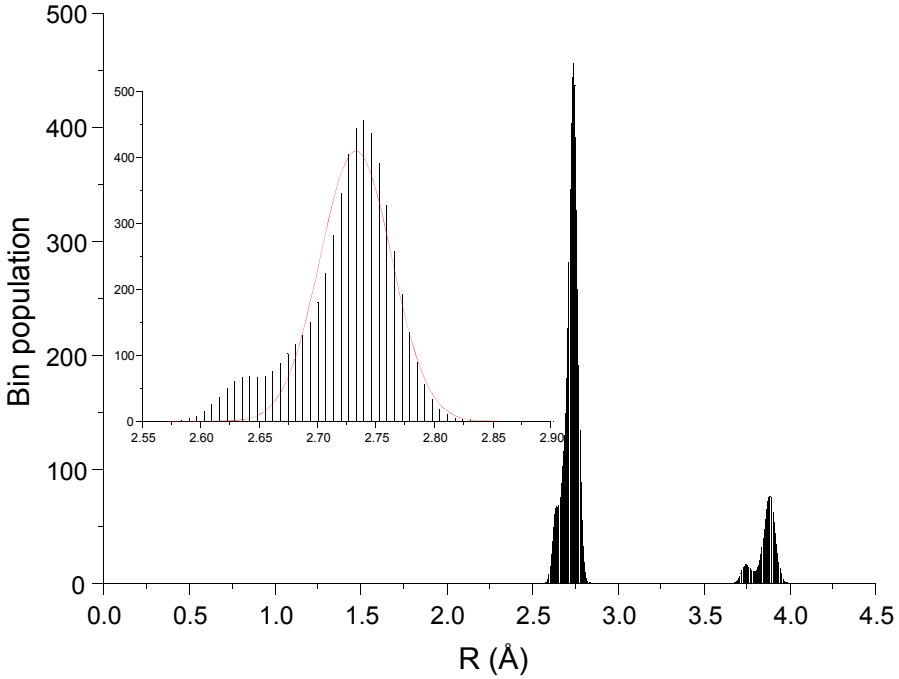

Figure 4: Sample histogram generated from Sutton-Chen MD output of a 381 atom Pt cluster at 20 K, with Gaussian fit over first shell (red line - inset). Vertical lines represent the total bin population over a range of nearest neighbour bond distances, thereby forming a radial distribution function.

The Gaussian fit across the first shell in **Figure 4** cannot encompass all the scattering paths, as the distribution is clearly bimodal, with a large contribution to the signal at shorter than average bond lengths. These contributions are from nearest neighbour pairs that involve at least one edge or vertex atom (**Figure 5**), and to a lesser extent, atoms on the faces of the nanoparticle surface.

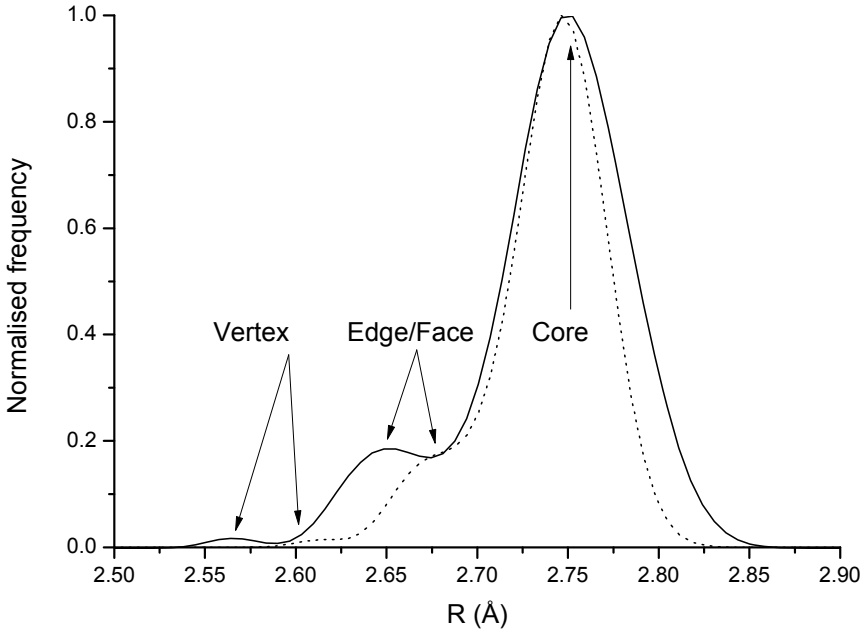

Figure 5: Origin of nearest neighbour pair contributions to histogram in 20 K simulations; Gupta potential (—) and Sutton-Chen potential (···).

As the cluster size increases, the core atom-pair contributions begin to dominate the RDF. As the number of core atoms decrease with decreasing size, the relative contributions of face and edge atoms increases. The contribution of the surface atoms to the first shell RDF is such that a single Gaussian distribution will no longer be able to accurately model the bond-length distribution in nanoparticles, highlighting the shortcomings of using a standard approach regarding EXAFS analysis of small nanoparticles. Thus, the attempts to fit a single peak over a bimodal distribution would require a larger σ^2 term to fit across the bond length distribution and result in a smaller path degeneracy (amplitude) than is actually the case. The average of the contracted surface bond length and the core bond length throughout the nanoparticle is measureable using the standard model, although due to the possible scale of surface contraction previously reported[13, 27], is unlikely to be representative of either.

V Results and Discussion

A XRD

XRD was used to identify which phases were present in the samples, and to determine crystallite size, although due to the size of the nanoparticles, the latter was for cross-correlation purposes rather than absolute size determination. XRD patterns of the 10-60 wt% Pt/C samples are presented in **Figure 6**.

The broad diffraction peak at approximately 25° due to the carbon support is observed in all patterns. The lowest loaded sample, 10 wt% (**Figure 6a**), exhibits a small amount of *fcc* crystalline Pt, although this is overlaid with some poorly crystalline tetragonal platinum oxide, most probably PtO, which remains in these as-prepared, i.e. not H_2 treated samples. The amount of "crystalline" Pt is too small to be resolved and the convolution of the broad diffraction peaks makes crystallite size determination unfeasible, highlighting a limitation of using XRD to characterise very small particles.

As the sample loading is increased to 20 wt% (**Figure 6b**), the corresponding slight increase in size is enough to make the poorly crystalline Pt detectable by XRD, with more appreciable amounts detectable for the 40 wt% and 60 wt% samples (**Figure 6c** and **6d**, respectively). The crystallite sizes were determined by a Rietveld analysis using TOPAS V3 software[42] and presented in **Table 1**. In all samples, there is still some poorly defined PtO present.

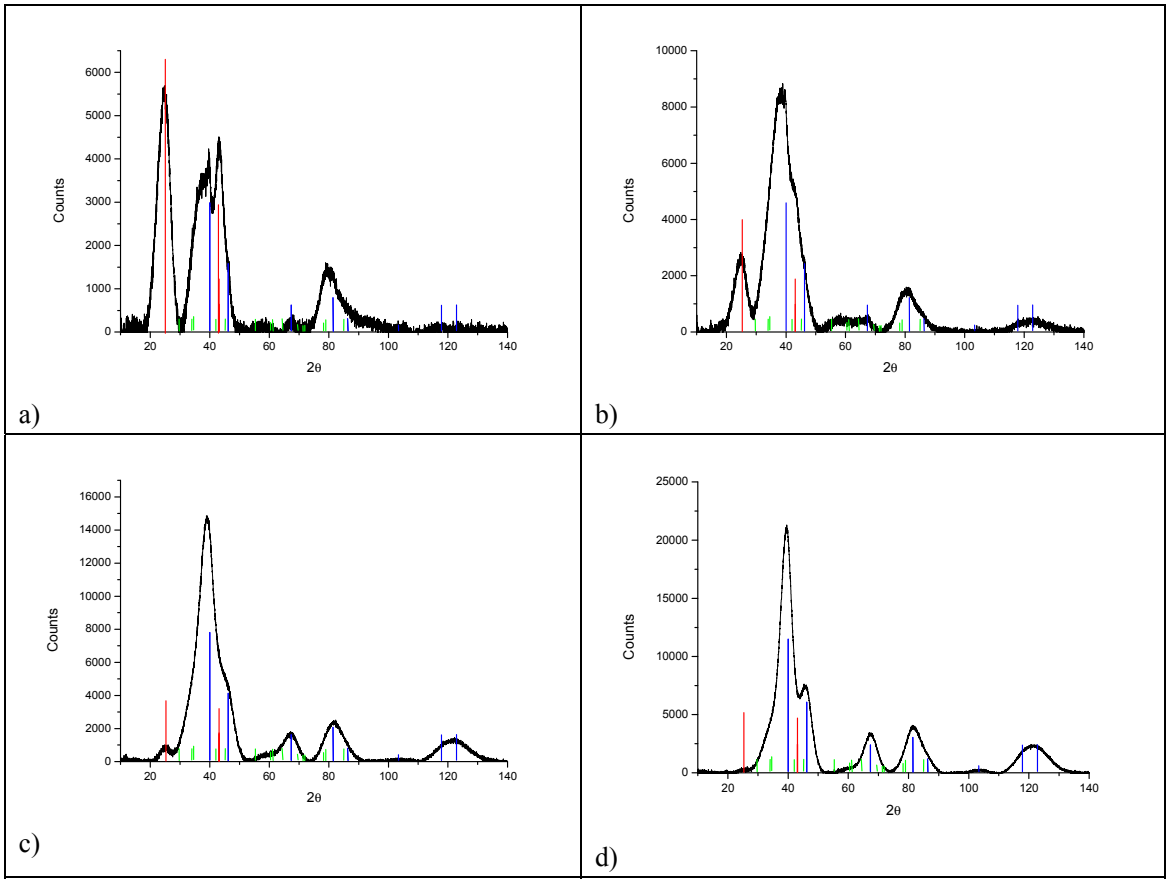

Figure 6: XRD patterns of a) 10 wt% Pt/C, b) 20 wt% Pt/C, c) 40 wt% Pt/C, and d) 60 wt% Pt/C. Data is the black line, | refers to cubic Pt (PDF No. 00-04-0802, a = 3.92 Å), | refers to tetragonal PtO (PDF No. 01-085-0714, a = 3.04 Å, c = 5.34 Å).

The presence of the poorly defined oxide phases hinders the calculation of crystallite size, as does the relatively high contribution from the carbon support for the lower loaded samples. Consequently, all crystallite sizes can only be regarded as approximations rather than absolute values.

Table 1: Cross correlation of average particle sizes determined by XRD, TEM and EXAFS analyses (XRD is Rietveld determined average crystallite size). XRD size determination was not possible for the 10 wt% sample due to very poor crystallinity. The TEM results are volume weighted and the error reported is the standard deviation of the particle size distribution. EXAFS particle size was determined based on the formulae of Jentys[40] and are the average of fits at 20, 150 and 300 K; the reported error is the variance.

Sample wt% Pt/C	Average particle size / nm						
	XRD	TEM		EXAFS			
	D_{Vol}	Particles observed	D_{Vol}	Standard	Cumulant	Gupta	Sutton-Chen
10	---	354	1.6 ± 0.5	1.5 ± 0.1	1.8 ± 0.4	2.1 ± 0.1	1.6 ± 0.1
20	1.5	445	2.4 ± 0.7	1.9 ± 0.3	2.1 ± 0.4	2.4 ± 0.6	2.0 ± 0.4
40	1.8	600	2.6 ± 0.7	2.3 ± 0.3	1.9 ± 0.3	3.0 ± 0.4	2.5 ± 0.3
60	2.3	433	3.0 ± 0.8	2.7 ± 0.3	2.0 ± 0.4	3.7 ± 0.5	2.9 ± 0.3

B TEM

TEM was used to give an indication of the average nanoparticle size and distribution in each sample. Micrographs were taken between 5 nm and 200 nm resolution; an example micrograph for each sample is given in **Figure 7** below.

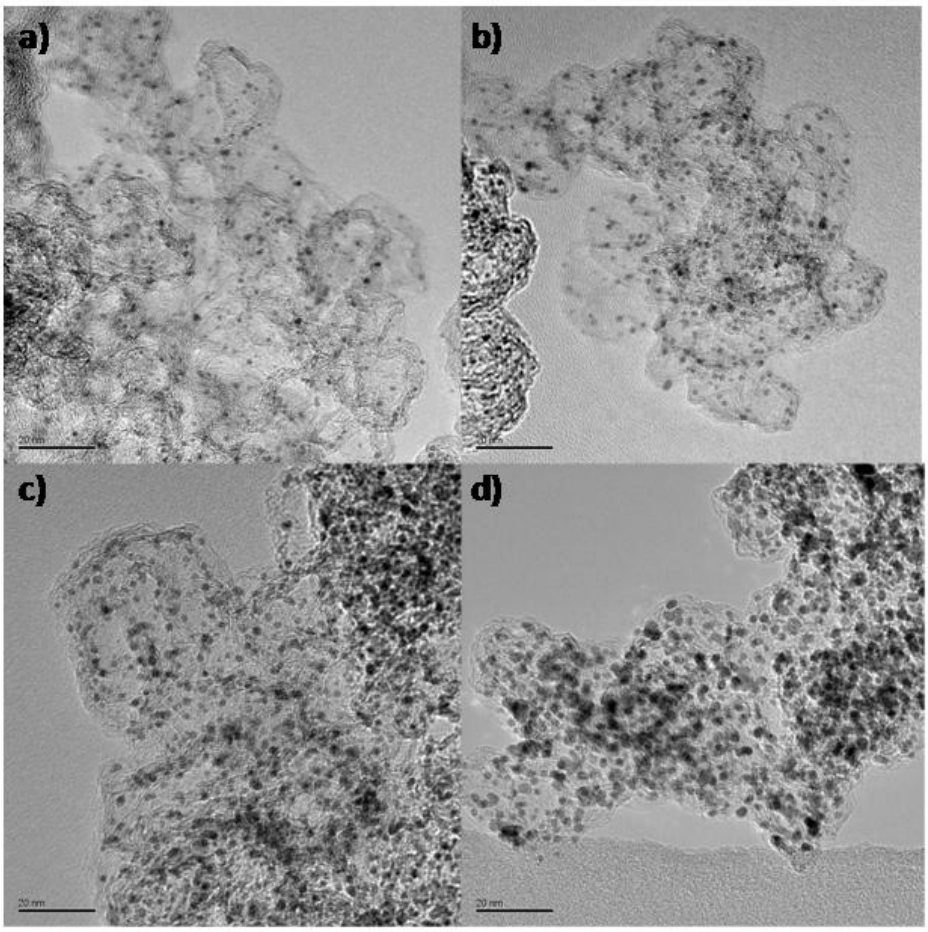

Figure 7: TEM micrographs of a) 10 wt% Pt/C, b) 20 wt% Pt/C, c) 40 wt% Pt/C and d) 60 wt% Pt/C. Scale bar is 20 nm.

Bright field (BF) micrographs at 10 and 20 nm scale were used for the particle size analysis (**Figure 8**), with between 350 and 600 particles being sampled. The samples all show the catalyst is well dispersed over the support, the distributions are all narrow, with small numbers of particles measured at either end of the distribution (**Table 1**). The narrow distribution and even dispersion suggest that the whole of each sample is uniform, which is useful for applying the MD-EXAFS method.

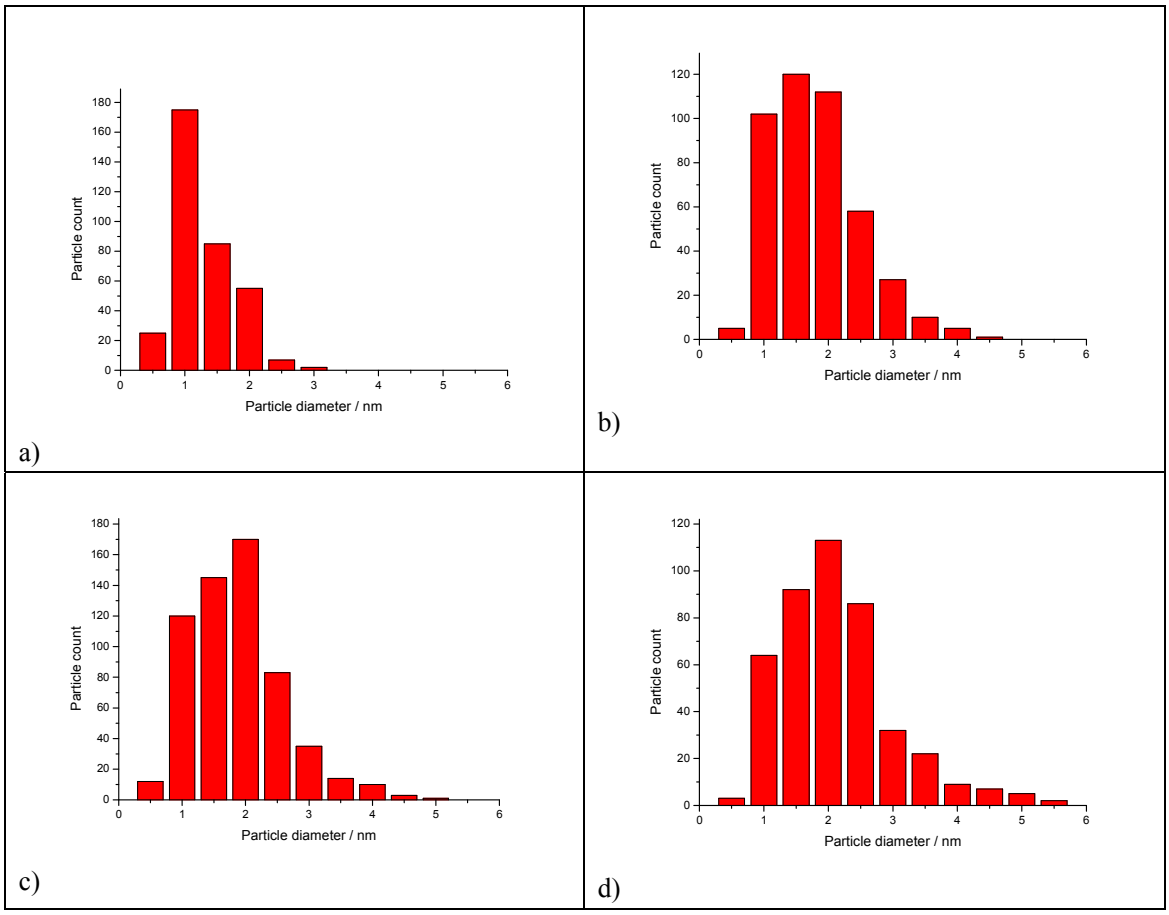

Figure 8: Particle size distribution determined by TEM of a) 10 wt% Pt/C, b) 20 wt% Pt/C, c) 40 wt% Pt/C and d) 60 wt% Pt/C.

In all cases the error (calculated as standard deviation) is less than a third of the average particle size, a result of the narrow size distribution. Analysis of the distribution from BF images is complicated by distinguishing the particles from the carbon support[43], as well as contrast between adjacent particles and overlap between particles in projection[44].

C EXAFS

1 Standard and cumulant approaches

In the analysis reported here, only the first coordination shell is analysed. Work is in progress to include higher coordination shells and multiple scattering paths in the MD-based EXAFS analysis. The fitted parameters using the standard method are reported in **Table 2**, and those using the higher cumulant approach in **Table 3**. The cumulant approach uses the standard approach as the basis for the fit, with the third and fourth cumulants as additional parameters. The R_f reported in the **Tables 2** and **3** is defined in **Equation 6**.

$$R_f = \frac{\sum_i (data_i - fit_i)^2}{\sum_i data_i^2}$$

Equation 6

The Rf is the sum of the square of the difference between the data and the fit at each data point divided by the sum of the square of the data at each data point, representing the mean square misfit between the data and the fit in both the imaginary and real parts of the Fourier transform[45].

Table 2: Structural parameters for 10 - 60 wt% Pt/C nanoparticles fit using the standard method at 20 K, 150 K and 300 K, acquired in a reduced H_2 environment at the Pt L_{III} edge.

Temperature	N	R	σ^2 / Å^{-2} ($\times 10^4$)	ΔE_0 / eV	R_f
10 wt% Pt/C					
20 K	7.89 ± 0.60	2.74 ± 0.01	50 ± 3	8.11 ± 0.70	0.009
150 K	7.91 ± 0.52	2.74 ± 0.01	61 ± 3	7.62 ± 0.63	0.009
300 K	8.23 ± 0.62	2.76 ± 0.01	71 ± 1	5.63 ± 0.69	0.017
20 wt% Pt/C					
20 K	8.24 ± 0.56	2.74 ± 0.01	55 ± 3	7.71 ± 0.59	0.009
150 K	8.41 ± 0.66	2.74 ± 0.01	62 ± 4	7.23 ± 0.72	0.014
300 K	8.88 ± 0.59	2.76 ± 0.01	68 ± 4	5.60 ± 0.62	0.015
40 wt% Pt/C					
20 K	9.37 ± 0.43	2.75 ± 0.01	35 ± 1	8.72 ± 0.50	0.004
150 K	8.96 ± 0.30	2.75± 0.01	46 ± 1	8.14 ± 0.29	0.002
300 K	8.70 ± 0.45	2.76 ± 0.01	62 ± 3	5.46 ± 0.52	0.010
60 wt% Pt/C					
20 K	9.64 ± 0.31	2.75 ± 0.01	42 ± 1	7.92 ± 0.29	0.002
150 K	9.40 ± 0.31	2.75 ± 0.01	46 ± 1	8.43 ± 0.34	0.002
300 K	9.04 ± 0.54	2.76 ± 0.01	59 ± 3	5.79 ± 0.62	0.010

Initially, looking at the quality of fit, the cumulant method appears to improve on the standard method as the R_f values are lower in most cases; however this would be expected on the addition of more variables to the fit. Of more importance is whether the values are physically reasonable, and how they compare with what is already known about the sample through other characterisation techniques.

The trends in coordination number and disorder for the cumulant analysis (**Table 3**) are less clear than those for standard analysis of the first coordination shell (**Table 2**). One cause of this is the inclusion of the fourth cumulant, C_4. In the majority of fits C_4 is negative and resulting in a flattening of the EXAFS signal (**Equation 5**, **Figure 1b**) and a corresponding decrease in the apparent coordination number for all the samples and an irregular temperature dependence of the disorder for the smaller two. Consequently, the particle size determined by the cumulant method differs from the standard method (**Table 1**). The third cumulant, C_3, increases with increasing measurement temperature as expected, although the increase is not linear and has large errors associated with it. C_3 is correlated with bond length, such that including a large positive C_3 results in a longer measured bond length, while a negative C_3 results in a shorter the bond length[7]. Whilst the bond distances reported in **Table 3** are reasonable, the consistency of the bond lengths obtained are not in good agreement with the large variation of C_3. Overall, the addition of C_3 and C_4 terms to the fit provide inconsistent results (**Table 3**), in that the results no longer follow the trends in particle size observed by XRD, TEM, and the standard EXAFS analysis (**Table 1**).

Table 3: Structural parameters for 10 - 60 wt% Pt/C nanoparticles fit using higher cumulants at 20 K, 150 K and 300 K, acquired in a reduced H_2 environment at the Pt L_{III} edge.

Temperature	N	R / Å	σ^2 *10^4/ Å^2	C_3 / Å^3 (×10^5)	C_4 / Å^4 (×10^6)	ΔE_0 / eV	R_f
				10 wt% Pt/C			
20 K	8.70 ± 0.83	2.73 ± 0.01	61 ± 9	-9.5 ± 5.0	12.7 ± 9.9	6.92 ± 0.82	0.004
150 K	8.76 ± 0.76	2.73 ± 0.01	73 ± 9	-8.1 ± 5.4	15.1 ± 10.7	6.74 ± 0.72	0.004
300 K	7.61 ± 0.93	2.76 ± 0.01	60 ± 14	115.8 ± 9.3	-13.8 ± 19.1	6.62 ± 0.99	0.009
				20 wt% Pt/C			
20 K	8.84 ± 1.10	2.74 ± 0.01	64 ± 13	-2.1 ± 7.2	10.3 ± 14.4	7.40 ± 1.03	0.008
150 K	9.12 ± 1.28	2.73 ± 0.01	73 ± 15	-0.6 ± 9.1	13.4 ± 18.1	7.12 ± 1.16	0.012
300 K	8.22 ± 0.89	2.77 ± 0.01	58 ± 12	9.4 ± 8.0	-13.2 ± 16.3	6.40 ± 0.89	0.007
				40 wt% Pt/C			
20 K	8.92 ± 0.69	2.75 ± 0.01	31 ± 6	-3.9 ± 3.2	-4.7 ± 6.1	8.05 ± 0.70	0.002
150 K	8.68 ± 0.57	2.75 ± 0.01	43 ± 6	-0.1 ± 0.3	-4.0 ± 6.5	8.10 ± 0.57	0.002
300 K	8.02 ± 0.68	2.77 ± 0.01	51 ± 9	8.7 ± 5.5	-14.0 ± 11.1	6.48 ± 0.70	0.004
				60 wt% Pt/C			
20 K	9.13 ± 0.52	2.75 ± 0.01	36 ± 5	-0.1 ± 2.0	-6.1 ± 5.3	7.88 ± 0.50	0.001
150 K	8.82 ± 0.42	2.75 ± 0.01	39 ± 4	1.6 ± 2.4	-1.1 ± 0.6	8.64 ± 0.42	0.001
300 K	8.05 ± 0.58	2.77 ± 0.01	44 ± 8	7.6 ± 4.6	-18.0 ± 10.4	6.62 ± 0.61	0.003

In addition to a worse cross-correlation with the TEM and XRD data the cumulant approach has several limitations. Cumulant expansions are only accurate at low *k* values, as they diverge with increasing *k* values[11]. However, the lowest *k* data is inherently missing in EXAFS[46]. This creates a particular problem for cumulant expansion analysis of heavier metal nanoparticles such as the Pt series in this work, where the quality of structural information increases with useable *k* range. Cumulant expansions can work very well for the first coordination shell, but are limited as they break down when applied to higher coordination shells, as they cannot easily be applied to multiple scattering effects, nor to systems with mixed coordination shells[10, 11]. Thus, for systems with high structural disorder, when more structural information is needed beyond the first shell, and when more than one element is present in the nearest coordination shell, another means is needed to account for the disorder

2 Application of MD to EXAFS

The RDF data was extracted from the Pt simulations run at 20 K, 150 K and 300 K (simulation temperatures corresponding to the EXAFS experimental conditions), and that for the first shell is plotted in **Figure 9**.

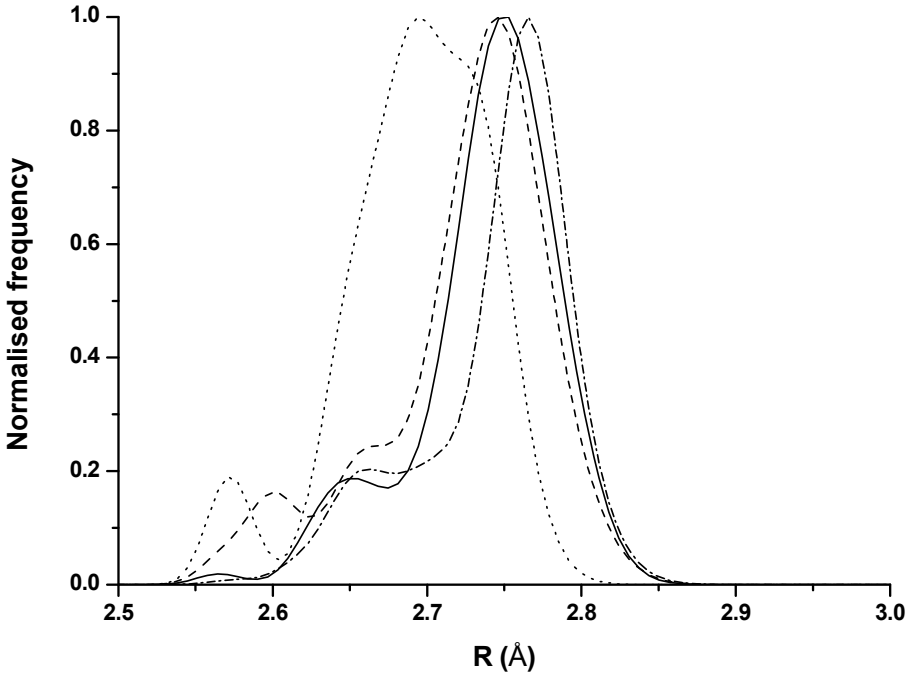

Figure 9: First shell RDFs at 20 K for 55 atom (····), 177 atom (----), 381 atom (—) and 767 atom (- · - ·) "spherical" Pt nanoparticles taken from MD simulations run using the Sutton Chen potential.

Each permutation of experimental temperature, MD simulation size and MD temperature was tried during the EXAFS analysis; the best fit results are in **Table 4** below. The 300 K simulations could not be fit to the data at all. As previously reported[34] the higher temperature simulations overestimate the disorder, requiring a negative σ^2 term to fit the data. Given this excessive disorder in the simulation these results were discounted. Simulations run at 150 K were able to be fit to data at 150 K and 300 K within the same error as the 20 K simulation (data not reported here). The smallest (55 atom) and largest (767 atom) simulated clusters had disorder that was too high and too low, respectively, and these too failed to give physically realistic fits to the data. All best reported fits are to the 381 atom cluster unless otherwise stated. Example fits for the 40 wt% Pt/C to the standard and MD models are included in **Figure 10**. The fits for the 10, 20 and 60 wt% Pt/C are included in the supplementary information (Figures S1-S3)[47].

Tables 4: Structural parameters for 10 - 60 wt% Pt/C nanoparticles fit using the MD method at 20 K, 150 K and 300 K, acquired in a reduced H_2 environment at the Pt L_{III} edge.

Temperature	Fitting method	N	α**	σ^2 / Å^{-2} ($\times 10^4$)	ΔE_0 / eV	R_f
			10 wt% Pt/C			
20 K	Gupta*	8.98 ± 0.39	-0.002 ± 0.001	31 ± 2	7.39 ± 0.28	0.004
	Sutton-Chen*	8.08 ± 0.44	0.002 ± 0.001	35 ± 2	7.58 ± 0.46	0.005
150 K	Gupta*	8.85 ± 0.39	-0.003 ± 0.001	41 ± 2	6.20 ± 0.40	0.004
	Sutton-Chen*	8.02 ± 0.29	0.001 ± 0.001	44 ± 2	7.23 ± 0.51	0.004
300 K	Gupta	8.67 ± 0.85	0.002 ± 0.002	54 ± 6	5.01 ± 0.80	0.023
	Sutton-Chen	8.31 ± 0.75	0.005 ± 0.001	60 ± 5	5.41 ± 0.66	0.015
			20 wt% Pt/C			
20 K	Gupta	8.64 ± 0.56	-0.004 ± 0.001	38 ± 3	6.90 ± 0.62	0.010
	Sutton-Chen	8.35 ± 0.54	-0.001 ± 0.001	45 ± 3	7.51 ± 0.56	0.008
150 K	Gupta	8.88 ± 0.67	-0.006 ± 0.001	45 ± 4	6.62 ± 0.74	0.015
	Sutton-Chen	8.53 ± 0.65	-0.003 ± 0.001	52 ± 4	7.05 ± 0.68	0.010
300 K	Gupta	9.67 ± 1.25	0.004 ± 0.002	52 ± 6	4.51 ± 1.01	0.016
	Sutton-Chen	9.15 ± 0.63	0.007 ± 0.001	58 ± 3	4.96 ± 0.63	0.010
			40 wt% Pt/C			
20 K	Gupta	10.02 ± 0.58	0.000 ± 0.000	19 ± 2	7.41 ± 0.62	0.005
	Sutton-Chen	9.52 ± 0.39	0.003 ± 0.001	25 ± 1	8.33 ± 0.37	0.003
150 K	Gupta	9.45 ± 0.55	-0.001 ± 0.001	29 ± 2	7.14 ± 0.53	0.003
	Sutton-Chen	9.08 ± 0.34	0.002 ± 0.001	36 ± 1	7.88 ± 0.35	0.002
300 K	Gupta	9.56 ± 1.27	0.002 ± 0.002	46 ± 6	4.66 ± 1.20	0.014
	Sutton-Chen	9.02 ± 0.65	0.005 ± 0.001	52 ± 3	5.34 ± 0.63	0.009
			60 wt% Pt/C			
20 K	Gupta	10.46 ± 0.79	-0.001 ± 0.001	26 ± 3	6.72 ± 0.73	0.003
	Sutton-Chen	9.85 ± 0.40	0.003 ± 0.001	31 ± 1	7.49 ± 0.44	0.001
150 K	Gupta	9.91 ± 0.68	-0.001 ± 0.001	29 ± 3	7.36 ± 0.67	0.009
	Sutton-Chen	9.60 ± 0.44	0.003 ± 0.001	36 ± 2	8.10 ± 0.41	0.002
300 K	Gupta	9.96 ± 1.31	0.003 ± 0.002	43 ± 6	4.81 ± 1.23	0.015
	Sutton-Chen	9.36 ± 0.68	0.007 ± 0.001	49 ± 3	5.39 ± 0.62	0.009

*177 atom cluster provided best fit

**A path length correction term (linear expansion coefficient α) was used as a fitting parameter for the MD input as well as the standard input. The very large number of paths contained in the MD input would make tabulated results of fitted bond lengths unwieldy, and as such the linear expansion coefficient is reported instead of the fitted bond length. For example an alpha of 0.003 moves the peak of the first shell distribution from 2.753 Å to 2.761 Å for the 381 atom cluster, and from 2.746 Å to 2.754 Å for the 177 atom cluster (using the Sutton Chen potential).

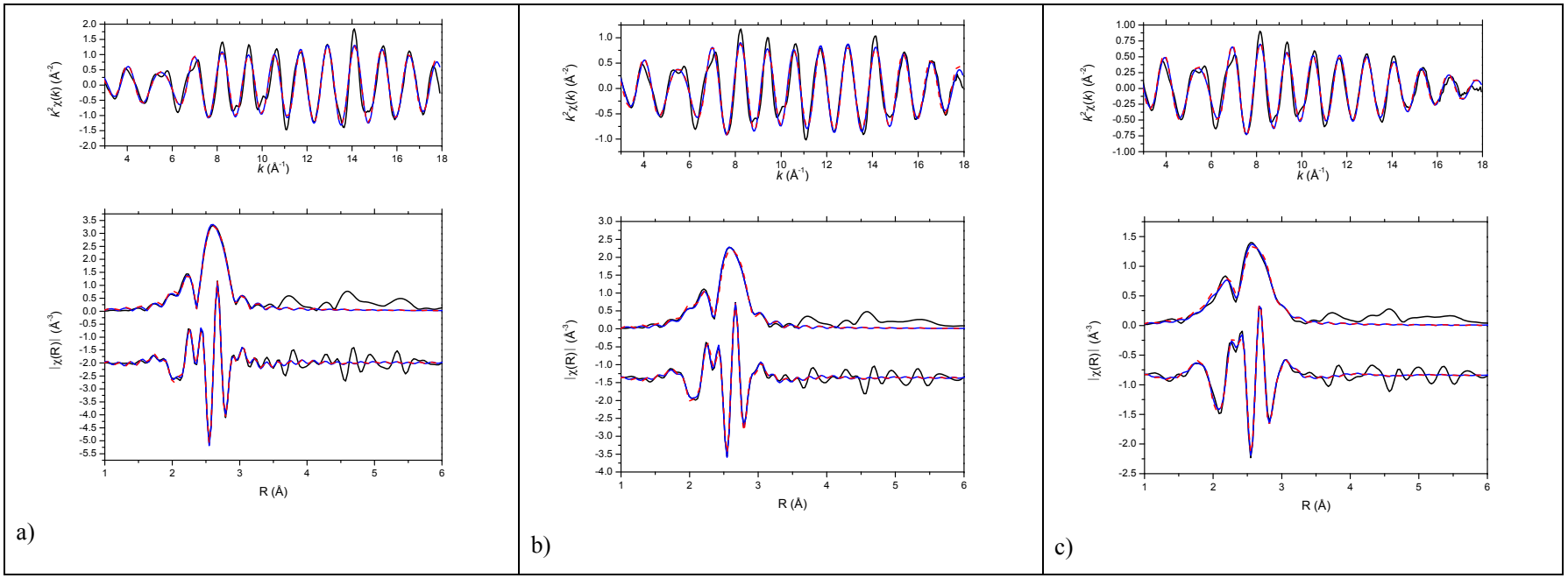

Figure 10: k^2 weighted experimental data (black) and fit to Standard (red) and Sutton-Chen (blue dashed) potentials, along with k^2 weighted magnitude and real Fourier transform for 40 wt% Pt/C at a) 20 K, b) 150 K and c) 300 K. The similarities in the visual fit are such that the two lines overlay.

The Sutton-Chen potential gave the best quality of fit, and the Gupta potential an inferior quality of fit (**Figure 11**) when compared with the standard fitting approach. This is attributed to the narrower distribution of bond lengths modelled by the Sutton-Chen potential; although the distribution still included a significant low *R* shoulder in the RDF due to surface contraction. The use of molecular dynamic simulations to fit real experimental data provides an improved fitting model as well as a measureable metric for evaluating the quality of a particular MD simulation or potential at replicating nanoparticle behaviour, bearing in mind the empirical potentials used in this work were designed to model bulk metal behaviour.

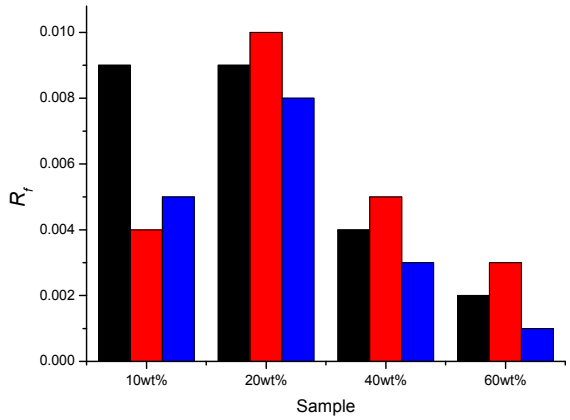

Figure 11: Comparison of quality of fit (R_f) to the first coordination shell between the standard fitting approach (black) and the applied molecular dynamic approaches; Gupta (red) and Sutton-Chen (blue). Fit is of simulation at 20 K to experimental data measured at 20 K.

As shown in the plots in both *k* and *R* space (supplementary information Figure S4)[47] there are no great differences between the fits using the two MD potentials. However, we conclude that the Sutton-Chen potential is superior to the Gupta potential in this case because of the consistently smaller R-factors and the generally smaller error bars. Thus, all the further results reported below will employ the Sutton-Chen potential.

Although the MD simulations provide an improved input for EXAFS analysis, resulting in a better fitting model, they do not completely account for all the structural and thermal (dynamic) disorder present in the measurements . The failure to accurately account for the disorder in an EXAFS measurement can lead to a reduction in the coordination number measured compared with its true value. The disorder required to fit the EXAFS using the standard approach is equivalent to the disorder required using the MD approach added to the disorder contained in the MD simulation. The additional disorder term was required for the MD fit as it is unlikely that any of the nanoparticles are the perfect "spheres" modelled, nor are they all of uniform size, and therefore the disorder contained in the simulations is not representative of the real sample. Accounting for the this by including an additional σ^2 parameter resulted in a further improvement to the fit results, producing consistently larger coordination numbers from the MD method than fits using the standard method at all the temperatures considered.

The magnitude of the increase in the coordination number was small, and within the generally accepted error limits[16] for coordination number determination. The coordination numbers determined

from the MD fits were converted into estimated average particle sizes and these are reported in **Table 1** alongside those from the standard fit for comparison. The MD method provides a more accurate fitting model than the standard method; whilst the coordination numbers and the derived particle sizes overlap within their error bars (Table 1), the MD method consistently gives larger coordination numbers over all the fits, with proportionately smaller errors and improved qualities (R_f) of fits over all samples and temperatures measured. When compared with TEM measurements, the MD approach gives a better agreement with regards to particle size, further illustrating the benefits of the MD approach compared to using theoretical models based on bulk samples when analysing the EXAFS of nanoparticles.

One interesting observation for the 10 wt% Pt/C sample at 20 K and 150 K was that the smaller 177 atom simulation provided a better fit than the 381 atom simulation. This simulation output (177 atoms) contained a greater degree of disorder than the larger simulation outputs. The difference between the fitted disorder using the MD simulation (vs. the standard method) was larger for these two measurements than all the others, yet the sum of the disorder within the MD simulation and the σ^2 required for the fit was equivalent to that of the standard fit. This is a validation of the MD method, with the smaller more disordered particles being fit best by smaller more disordered simulations and larger particles fit best by equivalent sized simulations. Also an encouraging result is that the sizes of MD simulation that provides the best fit for each particle size is in reasonable agreement with the TEM derived average particle sizes.

3 Effect of Histogram Bin Size

To understand whether the improved fit is more dependent on an increased number of scattering paths to parameterise the fit (i.e. the number of bins) or the location of the bins (i.e. the specific shape of the RDF brought about by different size simulated nanoparticles), the MD output histogram was re-binned. The initial set of simulations consisted of 0.0065 Å bin widths, giving a total of 1000 bins up to 6.5 Å i.e. up to and including the fourth nearest neighbour. This radial distance was chosen with the longer term goal of including multiple scattering effects in the MD fits. By fitting every permutation of RDF to experimental temperature, the effect of scattering path location and intensity was investigated, the results having already been discussed. To investigate the effect of the number of bins on the fit, the RDF histogram was re-binned with an order of magnitude more and less scattering paths, i.e. 100 total bins of 0.065 Å width and 10000 of 0.00065 Å width respectively. The standard EXAFS fitting procedure, based on a *fcc* lattice, defines a single distance and therefore only one single scattering path for the first nearest neighbour and can therefore be thought of in these terms as being a histogram effectively consisting of a single bin.

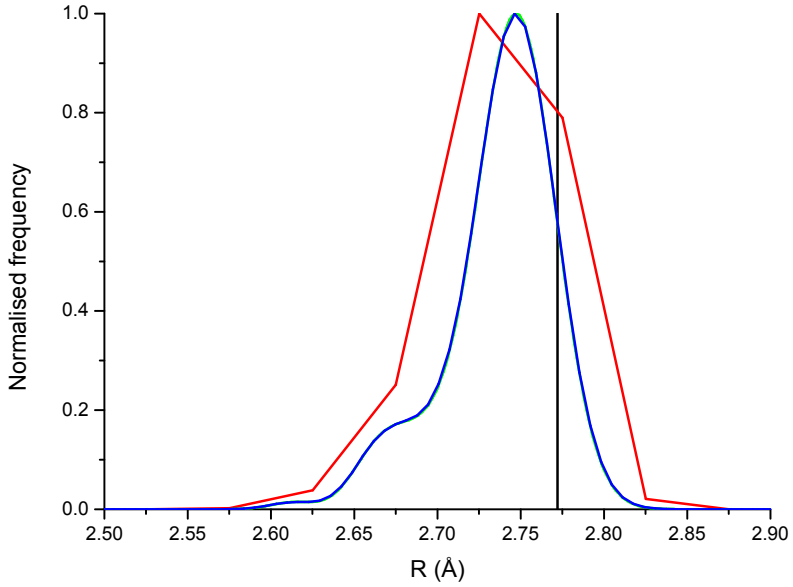

Figure 12: RDFs based on different histogram bin sizes; standard method (single bin)– black line; 0.065 Å bin size – red line, 0.0065 Å bin size – green line; 0.00065 Å bin size – blue line. The similarity of the lines for the two smallest bin sizes is such that they cannot be distinguished from one another.

Figure 12 shows how the histogram with the largest bin size has poorer spatial resolution, jumping roughly from bin to bin instead of the smooth variations observed for the 0.0065 Å and 0.00065 Å bin histograms. There is no visible difference in either plot (*k* or *R*) of the fits using different bin widths (**Figure 13**), as with using different potentials, but it is the quality of fit and evaluated parameters that indicate which model is best (**Table 5**). The coarse distribution provides the best first shell fit to the data. The MD fit converges with a relatively modest bin size, as the fits using 0.0065 Å and 0.00065 Å histogram bin widths produce numerically identical results and identical errors. A truer test of the effect of the number of histogram bins will be when more nearest neighbour shells are added to the fit, and multiple scattering contributions included.

Table 5: Effect of bin size on structural parameters for 20 wt% Pt/C nanoparticles at 20 K, acquired in a reduced H_2 environment at the Pt L_{III} edge.

Number of bins	*N*	*α*	σ^2 / Å^{-2} ($\times 10^4$)	ΔE_0 / eV	R_f
Standard	9.32 ± 0.42	-0.0068 ± 0.0006	35 ± 1	8.66 ± 0.45	0.0028
100 bin	9.40 ± 0.37	0.0041 ± 0.0005	22 ± 1	8.39 ± 0.40	0.0023
1000 bin	9.52 ± 0.39	0.0037 ± 0.0005	25 ± 1	8.26 ± 0.41	0.0025
10000 bin	9.52 ± 0.39	0.0037 ± 0.0005	25 ± 1	8.26 ± 0.41	0.0025

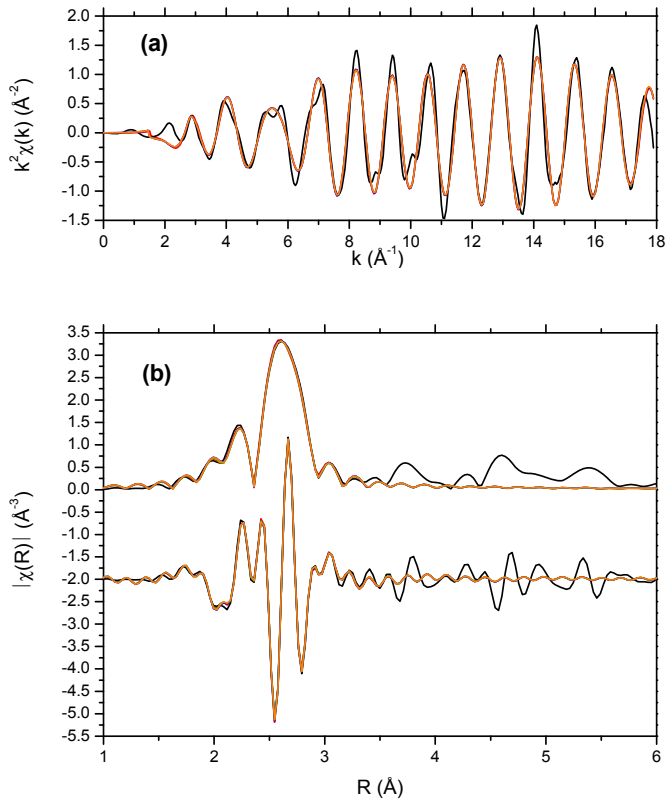

Figure 13: a) k^2 weighted experimental data and b) k^2 weighted magnitude and real Fourier transform for 40 wt% Pt/C at 20 K. Experimental data (black) fit to differing histogram bin sizes generated by Sutton-Chen potential; data – black line; standard (single bin)– red line; 0.065 Å bin size – green line, 0.0065 Å bin size – blue line; 0.00065 Å bin size – orange line. The similarity of the lines for each different fit is such that they cannot be distinguished from one another.

The change in quality of fit is marginal as a function of bin size, as are the differences in all parameters bar the coordination number, which shows a small increase for the smallest bin sizes. Bearing in mind the cross-correlation with TEM, the simulations resulting in the larger coordination numbers appear more physically reasonable at this stage, although the differences are within error values so no firm conclusion can be drawn until higher coordination shells are included in the MD fit.

VI Conclusions

The focus of this work has been to take on some of the more interesting challenges facing the analysis of EXAFS data for nanoparticles by combining molecular dynamic simulations with real experimental data. The contraction of the surface layer and anisotropic disorder of the surface atoms (brought about by their reduced coordination) were modelled using semi-empirical potentials, and the results successfully applied.

A full set of characterisation data is included in **Table 1** for cross-correlation purposes. The limitations of the higher cumulant approach to fitting nanoparticles have been exposed for systems

with these high levels of structural disorder, as is exhibited in the lack of trend in average particle diameter.

The use of MD to include anharmonic structural disorder in the EXAFS fit results in a larger average particle size that is in better agreement with TEM data than the standard approach. The new approach detailed in this work has shown promise. Extending the analysis to higher coordination shells would provide much more structural information. Work is in progress to extend this histogram approach both to higher shells and to three-body correlations incorporating the contributions from multiple-scattering paths.

The assumption of an unsupported "spherical" geometry is one limitation of the MD approach in its current form, as it can impose limitations on the relationship between coordination numbers in neighbouring coordination shells. This would likely become more apparent when extending the fit beyond the first nearest neighbour, and leads on to the next stage that could be attempted: modelling nanoparticles of other possible geometries such as icosahedral, cuboctahedral, or hemispherical; including a support in the simulations; and using the output from these expanded MD simulations for the EXAFS fit. Different geometries of nanoparticles have been simulated in many earlier studies[48-50], and the structural properties investigated. Similarly the different ratios between coordination shells have been investigated and the likely consequences this would have on the EXAFS[21, 41], however these studies have still assumed that each shell can be represented by a single bond length and a disorder term corresponding to a Gaussian distribution.

Determination of particle morphology from EXAFS would be indicated by an improved goodness of fit to the MD output from particular geometry, e.g. cuboctahedral. Whilst there are means of estimating particle morphology from EXAFS already from the population of the nearest neighbour coordination shells[40, 51], the errors reported for higher coordination shells are such that this method would not stand up by itself.

The analysis in this manuscript has been limited to the signal from the first coordination shell. The methodology presented for single scattering analysis is easily extended to higher coordination shells. However, consideration of higher shells requires a treatment of multiple scattering paths – particularly the various collinear contributing spectral weight at the same distance as the single scattering path from the fourth coordination shell. Handling such multiple scattering contributions within the context of the MD trajectories will be discussed in a future manuscript.

Although this manuscript presents an analysis of the EXAFS from mono-atomic nanoparticles using the results of a MD calculation, the methodology is readily extensible both to other materials and to other theories. The only aspect of the MD calculations used in this analysis was the listing of Cartesian coordinates of the atomic cluster at each time step. Any theory that provides a similar listing of Cartesian coordinates at one or more time points can be used as the input to this analytic approach. From the list of Cartesian coordinates, we extracted all Pt-Pt distances within a specified range of distances. To extend this approach to polyatomic clusters, we need only filter by scatterer species as well as by distance to construct histogram representations of the partial pair distributions about the absorbing atom. Thus the analytic approach presented here is broadly applicable. Any theory with structural output can be tested for consistency with measured EXAFS data using this approach.

Acknowledgements

The authors acknowledge the EPSRC and Johnson Matthey for funding and would like to thank Dr Brian Theobald and Dr Don Ozkaya of Johnson Matthey Technology Centre, Sonning Common for

supplying the catalysts samples, and for TEM measurements and analysis. The authors would also like to gratefully acknowledge Professor Gopinathan Sankar for useful discussions regarding the cumulant expansion method. N.Z. would like to thank the Southampton Nanoforum for a PhD studentship. C.-K.S would like to thank the Royal Society for a University Research Fellowship. Use of the National Synchrotron Light Source, Brookhaven National Laboratory, was supported by the U.S. Department of Energy, Office of Science, Office of Basic Energy Sciences, under Contract No. DE-AC02-98*C*H10886.

References

1 T. Shido and R. Prins, Journal of Physical Chemistry B **102**, 8426 (1998).
2 B. S. Clausen, L. Grabaek, H. Topsoe, L. B. Hansen, P. Stoltze, J. K. Norskov, and O. H. Nielsen, Journal of Catalysis **141**, 368 (1993).
3 B. S. Clausen, H. Topsøe, L. B. Hansen, P. Stoltze, and J. K. Nørskov, Catalysis Today **21**, 49 (1994).
4 E. Curis and S. Benazeth, Journal of Synchrotron Radiation **12**, 361 (2005).
5 S. Calvin, S. X. Luo, C. Caragianis-Broadbridge, J. K. McGuinness, E. Anderson, A. Lehman, K. H. Wee, S. A. Morrison, and L. K. Kurihara, Applied Physics Letters **87** (2005).
6 Y. Sun, et al., Langmuir **22**, 807 (2006).
7 E. Bus, J. T. Miller, A. J. Kropf, R. Prins, and J. A. van Bokhoven, Physical Chemistry Chemical Physics **8**, 3248 (2006).
8 P. Fornasini, F. Monti, and A. Sanson, Journal of Synchrotron Radiation **8**, 1214 (2001).
9 M. Bauer and H. Bertagnolli, Journal of Physical Chemistry B **111**, 13756 (2007).
10 G. Dalba and P. Fornasini, Journal of Synchrotron Radiation **4**, 243 (1997).
11 K. A. Daly and J. E. Penner-Hahn, Journal of Synchrotron Radiation **5**, 1383 (1998).
12 M. R. Martin and G. A. Somorjai, Physical Review B **7**, 3607 (1973).
13 W. J. Huang, R. Sun, J. Tao, L. D. Menard, R. G. Nuzzo, and J. M. Zuo, Nature Materials **7**, 308 (2008).
14 R. Smoluchowski, Physical Review **60**, 661 (1941).
15 L. Pauling, Journal of the American Chemical Society **69**, 542 (1947).
16 M. Vaarkamp, Catalysis Today **39**, 271 (1998).
17 B. S. Clausen, H. Topsoe, L. B. Hansen, P. Stoltze, and J. K. Norskov, Japanese Journal of Applied Physics Part 1-Regular Papers Short Notes & Review Papers **32**, 95 (1993).
18 G. Bunker, Nuclear Instruments & Methods **207**, 437 (1983).
19 E. C. Marques, D. R. Sandstrom, F. W. Lytle, and R. B. Greegor, The Journal of Chemical Physics **77**, 1027 (1982).
20 R. B. Greegor and F. W. Lytle, Journal of Catalysis **63**, 476 (1980).
21 A. I. Frenkel, Zeitschrift Fur Kristallographie **222**, 605 (2007).
22 J. M. Montejano-Carrizales, F. Aguilera-Granja, and J. L. Moran-Lopez, NanoStructured Materials **8**, 269 (1997).
23 A. M. Beale and B. M. Weckhuysen, Physical Chemistry Chemical Physics **12**, 5562 (2010).
24 Y. Okamoto, Nuclear Instruments and Methods in Physics Research Section A: Accelerators, Spectrometers, Detectors and Associated Equipment **526**, 572 (2004).
25 B. Gilbert, et al., Journal of Chemical Physics **120**, 11785 (2004).
26 P. Eisenberger and G. S. Brown, Solid State Communications **29**, 481 (1979).
27 A. Yevick and A. I. Frenkel, Physical Review B **81**, 115451 (2010).
28 B. Ravel, E. Cockayne, M. Newville, and K. M. Rabe, Physical Review B **60**, 14632 (1999).
29 B. Ravel, Y. I. Kim, P. M. Woodward, and C. M. Fang, Physical Review B **73** (2006).
30 W. Smith and T. R. Forester, Journal of Molecular Graphics **14**, 136 (1996).
31 B. Ravel, Journal of Synchrotron Radiation **8**, 314 (2001).
32 F. Cleri and V. Rosato, Physical Review B **48**, 22 (1993).
33 A. P. Sutton and J. Chen, Philosophical Magazine Letters **61**, 139 (1990).
34 O. M. Roscioni, N. Zonias, S. W. T. Price, A. E. Russell, T. Comaschi, and C.-K. Skylaris, Physical Review B **83**, 115409 (2011).

[35] B. Ravel and M. Newville, Journal of Synchrotron Radiation **12**, 537 (2005).
[36] J. J. Rehr, R. C. Albers, and S. I. Zabinsky, Physical Review Letters **69**, 3397 (1992).
[37] M. Newville, Journal of Synchrotron Radiation **8**, 96 (2001).
[38] M. Newville, P. Limacrvincedilscaron, Y. Yacoby, J. J. Rehr, and E. A. Stern, Physical Review B **47**, 14126 (1993).
[39] B. Ravel and S. D. Kelly, X-Ray Absorption Fine Structure-XAFS13 **882**, 150 (2007).
[40] A. Jentys, Physical Chemistry Chemical Physics **1**, 4059 (1999).
[41] R. E. Benfield, Journal of the Chemical Society-Faraday Transactions **88**, 1107 (1992).
[42] (Bruker, Karlsruhe, 2005), p. TOPAS V3
[43] D. Ozkaya, Platinum Metal Reviews **52**, 61 (2008).
[44] L. Cervera-Gontard and et al., Journal of Physics: Conference Series **26**, 367 (2006).
[45] S. D. Kelly, D. Hesterberg, and B. Ravel, in *Methods of Soil Analysis - Part 5. Mineralological Methods* (Soil Science Society of America, Madison, WI, 2008), p. 387.
[46] E. A. Stern, Y. Ma, O. Hanske-Petitpierre, and C. E. Bouldin, Physical Review B **46**, 687 (1992).
[47] See Supplemental Material at [URL] for data on further Pt/C samples and comparisons between different fitting models.
[48] G. D'Agostino, A. Pinto, and S. Mobilio, Physical Review B **48**, 14447 (1993).
[49] C. Mottet, J. Goniakowski, F. Baletto, R. Ferrando, and G. Treglia, Phase Transitions **77**, 101 (2004).
[50] B. C. Curley, R. L. Johnston, N. P. Young, Z. Y. Li, M. Di Vece, R. E. Palmer, and A. L. Bleloch, Journal of Physical Chemistry C **111**, 17846 (2007).
[51] P. V. Menacherry, M. Fernandez Garcia, and G. L. Haller, Journal of Catalysis **166**, 75 (1997).